

Virtual Compton Scattering in the Resonance Region up to the Deep Inelastic Region at Backward Angles and Momentum Transfer Squared of $Q^2 = 1.0 \text{ GeV}^2$

G. Laveissière,¹ N. Degrande,² S. Jaminion,¹ C. Jutier,^{1,3} L. Todor,³ R. Di Salvo,¹ L. Van Hoorebeke,² L.C. Alexa,⁴ B.D. Anderson,⁵ K.A. Aniol,⁶ K. Arundell,⁷ G. Audit,⁸ L. Auerbach,⁹ F.T. Baker,¹⁰ M. Baylac,⁸ J. Berthot,¹ P.Y. Bertin,¹ W. Bertozzi,¹¹ L. Bimbot,¹² W.U. Boeglin,¹³ E.J. Brash,⁴ V. Breton,¹ H. Breuer,¹⁴ E. Burtin,⁸ J.R. Calarco,¹⁵ L.S. Cardman,¹⁶ C. Cavata,⁸ C.-C. Chang,¹⁴ J.-P. Chen,¹⁶ E. Chudakov,¹⁶ E. Cisbani,¹⁷ D.S. Dale,¹⁸ C.W. de Jager,¹⁶ R. De Leo,¹⁹ A. Deur,^{1,16} N. d'Hose,⁸ G.E. Dodge,³ J.J. Domingo,¹⁶ L. Elouadrhiri,¹⁶ M.B. Epstein,⁶ L.A. Ewell,¹⁴ J.M. Finn,⁷ K.G. Fissum,¹¹ H. Fonvieille,¹ G. Fournier,⁸ B. Frois,⁸ S. Frullani,¹⁷ C. Furget,²⁰ H. Gao,¹¹ J. Gao,¹¹ F. Garibaldi,¹⁷ A. Gasparian,^{21,18} S. Gilad,¹¹ R. Gilman,^{22,16} A. Glamazdin,²³ C. Glashauser,²² J. Gomez,¹⁶ V. Gorbenko,²³ P. Grenier,¹ P.A.M. Guichon,⁸ J.O. Hansen,¹⁶ R. Holmes,²⁴ M. Holtrop,¹⁵ C. Howell,²⁵ G.M. Huber,⁴ C.E. Hyde-Wright,³ S. Incerti,⁹ M. Iodice,¹⁷ J. Jardillier,⁸ M.K. Jones,⁷ W. Kahl,²⁴ S. Kamalov,²⁶ S. Kato,²⁷ A.T. Katramatou,⁵ J.J. Kelly,¹⁴ S. Kerhoas,⁸ A. Ketikyan,²⁸ M. Khayat,⁵ K. Kino,²⁹ S. Kox,²⁰ L.H. Kramer,¹³ K.S. Kumar,³⁰ G. Kumbartzki,²² M. Kuss,¹⁶ A. Leone,³¹ J.J. LeRose,¹⁶ M. Liang,¹⁶ R.A. Lindgren,³² N. Liyanage,¹¹ G.J. Lolos,⁴ R.W. Lourie,³³ R. Madey,⁵ K. Maeda,²⁹ S. Malov,²² D.M. Manley,⁵ C. Marchand,⁸ D. Marchand,⁸ D.J. Margaziotis,⁶ P. Markowitz,¹³ J. Marroncle,⁸ J. Martino,⁸ K. McCormick,³ J. McIntyre,²² S. Mehrabyan,²⁸ F. Merchez,²⁰ Z.E. Meziani,⁹ R. Michaels,¹⁶ G.W. Miller,³⁰ J.Y. Mougey,²⁰ S.K. Nanda,¹⁶ D. Neyret,⁸ E.A.J.M. Offermann,¹⁶ Z. Papandreou,⁴ C.F. Perdrisat,⁷ R. Perrino,³¹ G.G. Petratos,⁵ S. Platchkov,⁸ R. Pomatsalyuk,²³ D.L. Prout,⁵ V.A. Punjabi,³⁴ T. Pussieux,⁸ G. Quémenér,^{1,7} R.D. Ransome,²² O. Ravel,¹ J.S. Real,²⁰ F. Renard,⁸ Y. Roblin,¹ D. Rowntree,¹¹ G. Rutledge,⁷ P.M. Rutt,²² A. Saha,¹⁶ T. Saito,²⁹ A.J. Sarty,³⁵ A. Serdarevic,^{4,16} T. Smith,¹⁵ G. Smirnov,¹ K. Soldi,³⁶ P. Sorokin,²³ P.A. Souder,²⁴ R. Suleiman,¹¹ J.A. Templon,¹⁰ T. Terasawa,²⁹ L. Tiator,²⁶ R. Tieulent,²⁰ E. Tomasi-Gustafsson,⁸ H. Tsubota,²⁹ H. Ueno,²⁷ P.E. Ulmer,³ G.M. Urciuoli,¹⁷ R. Van De Vyver,² R.L.J. Van der Meer,^{16,4} P. Vernin,⁸ B. Vlahovic,^{16,36} H. Voskanyan,²⁸ E. Voutier,²⁰ J.W. Watson,⁵ L.B. Weinstein,³ K. Wijesooriya,⁷ R. Wilson,³⁷ B.B. Wojtsekhowski,¹⁶ D.G. Zainea,⁴ W-M. Zhang,⁵ J. Zhao,¹¹ and Z.-L. Zhou¹¹

(The Jefferson Lab Hall A Collaboration)

¹Université Blaise Pascal/IN2P3, F-63177 Aubière, France

²University of Gent, B-9000 Gent, Belgium

³Old Dominion University, Norfolk, VA 23529

⁴University of Regina, Regina, SK S4S 0A2, Canada

⁵Kent State University, Kent OH 44242

⁶California State University, Los Angeles, Los Angeles, CA 90032

⁷College of William and Mary, Williamsburg, VA 23187

⁸CEA Saclay, F-91191 Gif-sur-Yvette, France

⁹Temple University, Philadelphia, PA 19122

¹⁰University of Georgia, Athens, GA 30602

¹¹Massachusetts Institute of Technology, Cambridge, MA 02139

¹²Institut de Physique Nucléaire, F-91406 Orsay, France

¹³Florida International University, Miami, FL 33199

¹⁴University of Maryland, College Park, MD 20742

¹⁵University of New Hampshire, Durham, NH 03824

¹⁶Thomas Jefferson National Accelerator Facility, Newport News, VA 23606

¹⁷INFN, Sezione Sanità and Istituto Superiore di Sanità, 00161 Rome, Italy

¹⁸University of Kentucky, Lexington, KY 40506

¹⁹INFN, Sezione di Bari and University of Bari, 70126 Bari, Italy

²⁰Laboratoire de Physique Subatomique et de Cosmologie, F-38026 Grenoble, France

²¹Hampton University, Hampton, VA 23668

²²Rutgers, The State University of New Jersey, Piscataway, NJ 08855

²³Kharkov Institute of Physics and Technology, Kharkov 61108, Ukraine

²⁴Syracuse University, Syracuse, NY 13244

²⁵Duke University, Durham, NC 27706

²⁶Institut fuer Kernphysik, University of Mainz, D-55099 Mainz, Germany

²⁷Yamagata University, Yamagata 990, Japan

²⁸Yerevan Physics Institute, Yerevan 375036, Armenia

²⁹Tohoku University, Sendai 980, Japan

³⁰Princeton University, Princeton, NJ 08544

³¹INFN, Sezione di Lecce, 73100 Lecce, Italy

³²University of Virginia, Charlottesville, VA 22901³³State University of New York at Stony Brook, Stony Brook, NY 11794³⁴Norfolk State University, Norfolk, VA 23504³⁵Florida State University, Tallahassee, FL 32306³⁶North Carolina Central University, Durham, NC 27707³⁷Harvard University, Cambridge, MA 02138

We have made the first measurements of the virtual Compton scattering process via the $ep \rightarrow ep\gamma$ exclusive reaction at $Q^2 = 1 \text{ GeV}^2$ in the nucleon resonance region. The cross section is obtained at center of mass (CM) backward angle, in a range of total (γ^*p) CM energy W from the proton mass up to $W = 1.91 \text{ GeV}$. The data show resonant structures in the first and second resonance regions, and are well reproduced at higher W by the Bethe-Heitler+Born cross section, including t -channel π^0 -exchange. At high W , our data, together with existing real photon data, show a striking Q^2 independence. Our measurement of the ratio of $H(e, e'p)\gamma$ to $H(e, e'p)\pi^0$ cross sections is presented and compared to model predictions.

PACS numbers: 13.60.-r, 13.60.Fz

Understanding nucleon structure in terms of the non-perturbative dynamics of quarks and gluons requires new and diverse experimental data to guide theoretical approaches and to constrain models. Purely electro-weak processes are privileged tools since they can be interpreted directly in terms of the current carried by the quarks. This Letter presents a study of the virtual Compton scattering (VCS) process: $\gamma^*p \rightarrow \gamma p$, in the nucleon resonance region via the photon electroproduction reaction: $H(e, e'p)\gamma$. For the first time, we separate this process from the dominant $H(e, e'p)\pi^0$ reaction above pion threshold.

The Constituent Quark Model of Isgur and Karl [1] reproduces many features of the nucleon spectrum. However, for $W > 1.6 \text{ GeV}$, the model predicts a number of positive parity resonances [2] that have not been seen experimentally. The simultaneous study of both ($N\pi$) and ($N\gamma$) final states of the electroproduction process on the nucleon offers probes with very different sensitivities to the resonance structures. Another motivation for the present study is to explore the exclusive $ep \rightarrow ep\gamma$ reaction at high W , where current quark degrees of freedom may become as important as those of constituent quarks in the understanding of resonances. Quark-hadron duality implies that even at modest Q^2 , inelastic electron scattering in the resonance region can be analyzed in terms of quark degrees of freedom in the t -channel of the forward Compton amplitude instead of nucleon resonances in the s -channel [3].

We define the kinematics of the $ep \rightarrow ep\gamma$ reaction in Fig. 1a. A common set of invariant kinematic variables is defined as $-Q^2 = (k - k')^2 = q^2$, $s = W^2 = (q + p)^2$, $t = (p - p')^2$, and $u = (p - q')^2$. The \vec{q} -direction defines the polar-axis of the coordinate system: $\theta_{\gamma\gamma}^*$ and $\phi_{\gamma\gamma}$ are the polar and azimuthal angles in the $\gamma^*p \rightarrow \gamma p$ subprocess CM frame. The scattered electron direction defines $\phi_{\gamma\gamma} = 0$. The $ep \rightarrow ep\gamma$ reaction was measured below pion threshold at MAMI ($Q^2 = 0.33 \text{ GeV}^2$) [5] and at the Thomas Jefferson National Accelerator Facility (JLab) ($Q^2 = 0.92$ and 1.76 GeV^2) [6]. We present

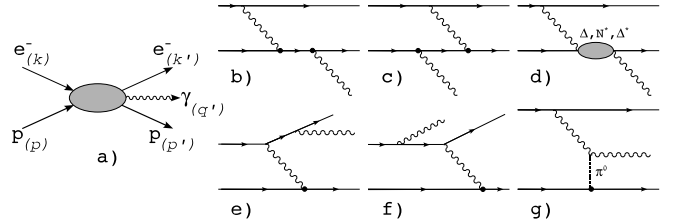


FIG. 1: Kinematics for photon electroproduction on the proton (a) and lowest order amplitudes for VCS Born (b, c), VCS Non-Born (d), Bethe-Heitler (e, f) and t -channel π^0 -exchange (g) [4] processes. The particles 4-momenta are indicated in parenthesis.

in this letter the first measurements of the nucleon excitation up to $W = 1.91 \text{ GeV}$ at $Q^2 = 1 \text{ GeV}^2$ through the $ep \rightarrow ep\gamma$ process in CM backward kinematics (\vec{q}' opposite to \vec{q}).

In the one photon exchange approximation, the $ep \rightarrow ep\gamma$ amplitude (Fig. 1a) includes the coherent superposition of the VCS Born (Fig. 1b and 1c) and Non-Born (Fig. 1d) amplitudes, and the Bethe-Heitler (BH) amplitude (Fig. 1e and 1f) [7]. Note that in the BH amplitude, the mass of the virtual photon (elastically absorbed by the proton) is t . In the VCS amplitude, the mass of the virtual photon (inelastically absorbed) is $-Q^2$. The BH amplitude dominates over the VCS when the photon is emitted in either the direction of the incident or scattered electron, and breaks the symmetry of the electroproduction amplitude around the virtual photon direction. Thus, it is not possible to expand the $\phi_{\gamma\gamma}$ -dependence of the $ep \rightarrow ep\gamma$ cross section in terms of the usual electroproduction LT and TT interference terms, except when the BH amplitude is really negligible. Above the Δ -resonance, the VCS amplitude is the dominant contribution in our kinematics. In this region, the data are $\phi_{\gamma\gamma}$ -independent, within our statistics. For these reasons, we have not performed azimuthal analysis of the data.

The experiment was performed at JLab in Hall A. The

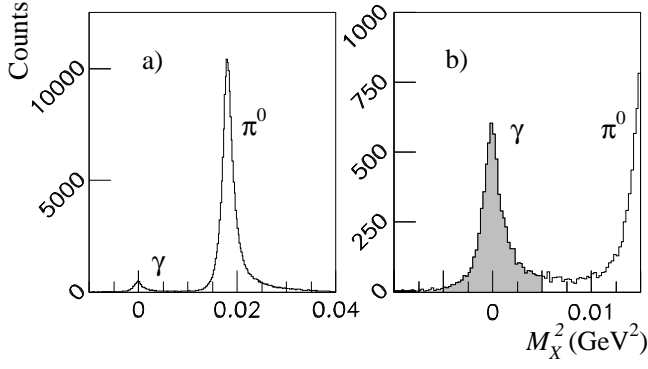


FIG. 2: Squared missing mass M_X^2 for an experimental setting at $W = 1.2$ GeV (a) and zoom around the γ peak (b). The shaded window $[-0.005, 0.005$ GeV^2] is used to select the γ events.

continuous electron beam of energy 4.032 GeV with an intensity of 60-120 μA bombarded a 15 cm liquid hydrogen target. The scattered electron and recoil proton were detected in coincidence in two high resolution spectrometers. The emitted photon was reconstructed using a missing particle technique. A spectrum of the squared missing mass $M_X^2 = (k+p-k'-p')^2$ is displayed in Fig 2. We give a detailed description of the apparatus, detector acceptance, and systematic errors in [8], [9] and [10].

We extract the 5-fold differential cross section $d^5\sigma = d^5\sigma/dk'_{lab}d[\Omega_e]_{lab}d[\Omega_p]_{CM}$ using the method described in [9]; dk'_{lab} and $d[\Omega_e]_{lab}$ are the scattered electron differential momentum and solid angle in the lab frame, and $d[\Omega_p]_{CM}$ is the proton CM differential solid angle. The calculations of the solid angle and radiative corrections are based on a simulation [11] including the coherent sum of the BH and VCS-Born amplitudes (Fig. 1b, c, e and f) only. The inclusion of the BH-amplitude ensures that our simulation reproduces the strong $\phi_{\gamma\gamma}$ dependence near threshold. Corrections were applied for acceptance, trigger efficiency, acquisition and electronic dead times, tracking efficiency, target boiling, target impurity and proton absorption [9]. In addition, the correction (-0.1 to -1.7%) for exclusive π^0 background in the M_X^2 window $[-0.005, 0.005]$ GeV^2 was made using our simulation [9]. The main results are displayed in Fig. 3, 4 and 5. On these figures, errors are statistical only; the systematic errors are of the same order.

In Fig. 3 we present the 5-fold differential cross sections $d^5\sigma$ for the six bins in $\phi_{\gamma\gamma}$ (30° wide) as a function of W , at $Q^2 = 1$ GeV^2 and $\cos\theta_{\gamma\gamma}^* = -0.975$. By symmetry, the statistics from $\phi_{\gamma\gamma} = 0$ to -180° are also included. The cross sections we obtain are displayed in tables I, II and III. Note that these tables are not completely filled due to the acceptance of the experiment. The data show strong resonance phenomena in the first and second resonance regions, but the higher resonances are not distinguishable due to the limited statistical precision.

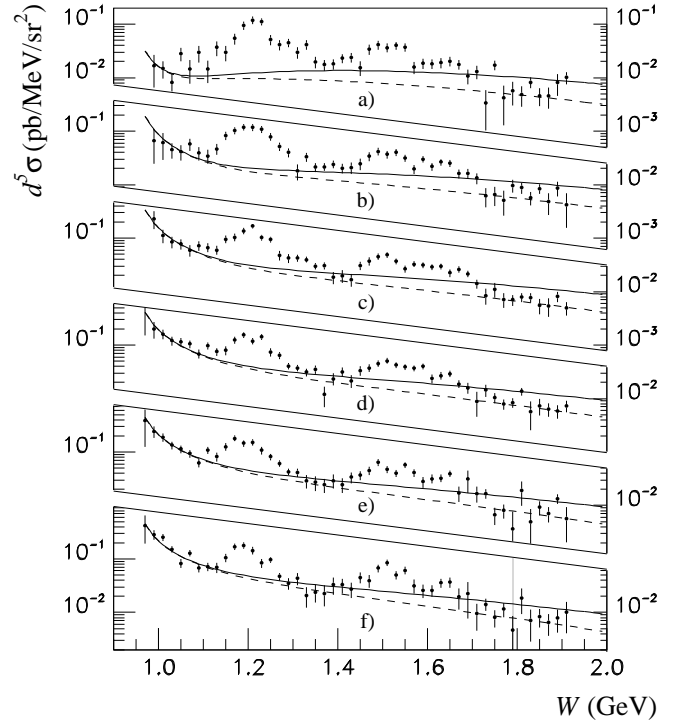


FIG. 3: Excitation curves for $ep \rightarrow ep\gamma$ at $Q^2 = 1$ GeV^2 , $\cos\theta_{\gamma\gamma}^* = -0.975$ and $\phi_{\gamma\gamma} = 15^\circ$ (a), 45° (b), 75° (c), 105° (d), 135° (e) and 165° (f). The full line is the BH+Born cross section, and the dashed line is the BH+Born+ π^0 -exchange cross section [4] (see text).

The VCS data in Fig: 3 approach the BH+Born calculation at high W , when we include the destructive t -channel π^0 exchange graph [4] of Fig. 1g). In the resonance model of Capstick and Keister [12], the positive parity intermediate states contribute constructively and the negative parity states contribute destructively to the backward angle cross section. If there are no diffractive minima as a function of Q^2 , this effect will remain in VCS. As the level density grows with W , the positive and negative parity resonances tend to compensate and the backward cross section decreases with increasing W .

Real Compton scattering (RCS) has been intensively investigated in the $\Delta(1232)$ -resonance [13] and in the high energy diffractive region [14]. RCS was also studied above the $\Delta(1232)$ at Bonn [15], Saskatoon [16], and Tokyo [17, 18]. The Cornell experiment [19] measured the RCS process at photon energies E_γ in the range 2–6 GeV and angles from 45° to 128° in the CM frame. The recent JLab experiment E99-114 measured the RCS process at E_γ in the range 3–6 GeV. We note that the large angle RCS data are roughly independent of angle for $\theta_{\gamma\gamma}^* > 90^\circ$. The Cornell RCS data (W , $-t$, $-u$ all large) are qualitatively consistent with the s^{-6} scaling law for $d\sigma/dt$ [20] or with a t -dependent Compton form factor [21, 22, 23]. In Fig. 4, we compare our backward angle $ep \rightarrow ep\gamma$ cross section divided by the photon flux factor (Hand

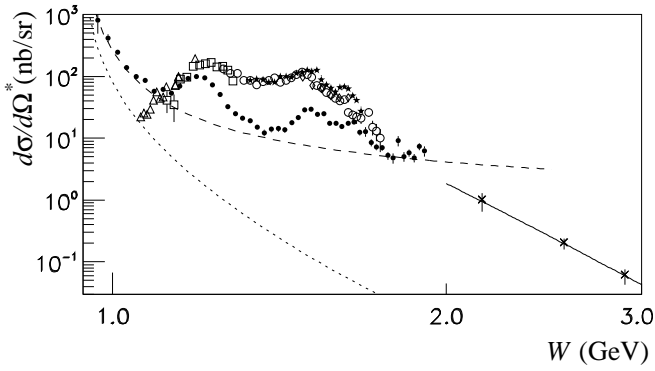


FIG. 4: Comparison of VCS data from this experiment (\bullet) at $\theta_{\gamma\gamma}^* = 167.2^\circ$ and RCS data at $\theta_{\gamma\gamma}^* = 159 - 162^\circ$ (\star) [17], $\theta_{\gamma\gamma}^* = 128 - 132^\circ$ (\diamond) [15], $\theta_{\gamma\gamma}^* = 141^\circ$ (\triangle) [16], $\theta_{\gamma\gamma}^* = 130 - 133^\circ$ (\circ) [18], $\theta_{\gamma\gamma}^* = 131^\circ$ (\square) [13] and $\theta_{\gamma\gamma}^* = 105 - 128^\circ$ (\times) [19]. The solid curve is an s^{-6} power law normalized to the $W = 2.55$ GeV Cornell point. The dashed curve is the BH+Born+ π^0 -exchange cross section (see text) and the dotted curve the BH alone.

convention [9]) with existing large angle RCS data. For comparison purposes, we average our VCS cross sections over the azimuthal angle $\phi_{\gamma\gamma}$.

In the resonance region, the VCS/RCS comparison in Fig. 4 shows a strong decrease with Q^2 as expected from resonance form factors. This is in contrast with the behavior in the region of $W \sim 1.8$ GeV where our VCS data are approximately equal to the wide angle RCS data. This evidence of Q^2 -independence suggests that the Compton process is coupling to point-like constituents. This conjecture can be tested with new backward angle VCS data at large W and at this Q^2 and above. If this Q^2 -independence is confirmed, we emphasize that this is a new probe of the quark structure of the proton.

From these results and those presented in [9], we have computed the ratio between the $ep \rightarrow ep\gamma$ and $ep \rightarrow ep\pi^0$ cross sections at $\cos\theta_{\gamma\gamma}^* = -0.975$ and $Q^2 = 1$ GeV 2 for the entire resonance region. In Fig. 5 we show the value of the ratio averaged over the six bins in $\phi_{\gamma\gamma}$. In the region of the P_{33} Δ -resonance, the experimental ratio is five times larger than the BH+Born+ π^0 -exchange cross section divided by the MAID2003 [24] calculation. Thus one has to be careful when correcting $H(e, e'p)\pi^0$ experiments if the resolution does not allow a clear separation of the $H(e, e'p)\gamma$ channel.

In summary, we studied for the first time the process $ep \rightarrow ep\gamma$ in the nucleon resonance region. The data is dominated by the VCS process and show similar resonance phenomena as for RCS. At high W the Q^2 independence of the data suggest the VCS process is coupling to elementary quarks. The comparison with $ep \rightarrow ep\pi^0$ shows strong variations with W across the resonance region.

We wish to acknowledge essential work of the JLab

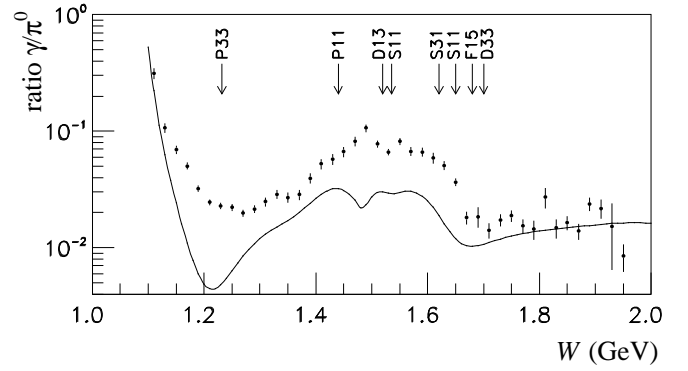


FIG. 5: Ratio of $ep \rightarrow ep\gamma$ over $ep \rightarrow ep\pi^0$ cross sections at $Q^2 = 1$ GeV 2 and $\theta_{\gamma\gamma}^* = 167.2^\circ$. The full curve is the ratio between the BH+Born+ π^0 -exchange cross section and the MAID2003 model [24].

accelerator staff and Hall A technical staff. This work was supported by DOE contract DE-AC05-84ER40150 under which the Southeastern Universities Research Association (SURA) operates the Thomas Jefferson National Accelerator Facility. We acknowledge additional grants from the US DOE and NSF, the French Centre National de la Recherche Scientifique and Commissariat à l'Énergie Atomique, the Conseil Régional d'Auvergne, the FWO-Flanders (Belgium) and the BOF-Gent University.

-
- [1] N. Isgur and G. Karl, Phys. Rev. **D19**, 2653 (1979).
 - [2] R. Koniuk and N. Isgur, Phys. Rev. Lett. **44**, 845 (1980).
 - [3] I. Niculescu et al., Phys. Rev. Lett. **85**, 1186 (2000).
 - [4] M. Vanderhaeghen, Phys. Lett. **B368**, 13 (1996).
 - [5] J. Roche et al., Phys. Rev. Lett. **85**, 708 (2000).
 - [6] G. Laveissiere et al., Phys. Rev. Lett. **93**, 122001 (2004).
 - [7] H. Bethe and W. Heitler, Proc. Roy. Soc. Lond. **A146**, 83 (1934).
 - [8] J. Alcorn et al., Nucl. Instrum. Meth. **A522**, 294 (2004).
 - [9] G. Laveissiere et al., Phys. Rev. **C69**, 045203 (2004).
 - [10] G. Laveissiere, Ph.D. thesis, Université Blaise Pascal, Clermont-Fd, France (2001), DU 1309.
 - [11] L. Van Hoorebeke et al., to be submitted to NIM A.
 - [12] S. Capstick and B. D. Keister, Phys. Rev. **D47**, 860 (1993), and Phys. Rev. **D46**, 84 (1992).
 - [13] F. Wissmann et al., Nucl. Phys. **A660**, 232 (1999).
 - [14] T. H. Bauer, R. D. Spital, D. R. Yennie, and F. M. Pipkin, Rev. Mod. Phys. **50**, 261 (1978).
 - [15] M. Jung et al., Zeit. Phys. **C10**, 197 (1981).
 - [16] E. L. Hallin et al., Phys. Rev. **C48**, 1497 (1993).
 - [17] Y. Wada et al., Nucl. Phys. **B247**, 313 (1984).
 - [18] T. Ishii et al., Nucl. Phys. **B254**, 458 (1985).
 - [19] M. A. Shupe et al., Phys. Rev. **D19**, 1921 (1979).
 - [20] S. J. Brodsky and G. R. Farrar, Phys. Rev. **D11**, 1309 (1975).
 - [21] A. V. Radyushkin, Phys. Rev. **D58**, 114008 (1998).
 - [22] H. W. Huang, P. Kroll, and T. Morii, Eur. Phys. J. **C23**, 301 (2002).

TABLE I: $ep \rightarrow ep\gamma$ cross section (\pm stat \pm syst) at $Q^2=1.0$ GeV² and $\cos\theta_{\gamma\gamma}^* = -0.975$, in fm/MeV/sr².

$W(\text{GeV})$	$\phi = 15^\circ$	$\phi = 45^\circ$	$\phi = 75^\circ$	$\phi = 105^\circ$	$\phi = 135^\circ$	$\phi = 165^\circ$
0.99	16.6 \pm 10.1 \pm 6.3	66 \pm 41 \pm 93	231 \pm 84 \pm 101	200 \pm 70 \pm 77	243 \pm 59 \pm 108	288 \pm 59 \pm 104
1.01	14.9 \pm 5.4 \pm 5.6	61 \pm 32 \pm 36	111 \pm 30 \pm 20	161 \pm 33 \pm 30	188 \pm 34 \pm 64	254 \pm 35 \pm 45
1.03	8.1 \pm 4.1 \pm 4.3	45.2 \pm 14.9 \pm 6.4	85 \pm 21 \pm 14	119 \pm 22 \pm 24	134 \pm 22 \pm 20	152 \pm 22 \pm 33
1.05	28.4 \pm 8.3 \pm 4.7	41 \pm 13 \pm 15	77 \pm 17 \pm 23	114 \pm 19 \pm 23	114 \pm 18 \pm 15	83 \pm 15 \pm 62
1.07	14.6 \pm 6.8 \pm 4.0	57.6 \pm 14.8 \pm 9.2	59 \pm 13 \pm 13	104 \pm 17 \pm 18	94 \pm 15 \pm 25	128 \pm 17 \pm 24
1.09	29.5 \pm 10.2 \pm 4.2	39 \pm 10 \pm 10	71.9 \pm 14.2 \pm 9.8	68 \pm 12 \pm 10	63 \pm 11 \pm 12	67 \pm 12 \pm 24
1.11	14.4 \pm 6.4 \pm 5.0	34.6 \pm 10.0 \pm 2.8	66.9 \pm 12.8 \pm 9.2	97 \pm 14 \pm 11	109.4 \pm 16.5 \pm 9.4	71 \pm 13 \pm 18
1.13	36.7 \pm 11.2 \pm 7.7	46.4 \pm 10.6 \pm 7.3	59 \pm 11 \pm 15	75.1 \pm 13.1 \pm 9.0	82 \pm 15 \pm 17	69.5 \pm 15.7 \pm 3.9
1.15	30.0 \pm 9.6 \pm 15.9	82 \pm 14 \pm 15	95.7 \pm 15.1 \pm 9.3	79 \pm 14 \pm 14	125 \pm 20 \pm 43	105 \pm 18 \pm 27
1.17	54.1 \pm 12.9 \pm 9.5	103.1 \pm 16.1 \pm 8.9	104 \pm 17 \pm 12	124.4 \pm 17.5 \pm 9.3	180 \pm 22 \pm 24	168 \pm 22 \pm 10
1.19	94.3 \pm 16.4 \pm 7.5	118 \pm 17 \pm 13	135 \pm 17 \pm 13	154 \pm 18 \pm 23	145 \pm 19 \pm 14	178 \pm 24 \pm 15
1.21	119 \pm 18 \pm 17	117 \pm 16 \pm 20	167.8 \pm 18.3 \pm 9.1	119 \pm 15 \pm 10	153.0 \pm 21.0 \pm 6.7	144 \pm 24 \pm 20
1.23	111 \pm 16 \pm 13	108 \pm 15 \pm 18	102 \pm 13 \pm 11	141.6 \pm 16.8 \pm 8.0	107 \pm 17 \pm 18	83 \pm 15 \pm 14
1.25	51 \pm 11 \pm 12	78 \pm 12 \pm 11	94 \pm 12 \pm 11	74 \pm 13 \pm 10	81.3 \pm 11.8 \pm 6.7	96 \pm 12 \pm 10
1.27	41.3 \pm 9.2 \pm 7.1	51.5 \pm 9.3 \pm 6.3	48.1 \pm 9.8 \pm 6.9	64.4 \pm 9.5 \pm 4.1	61.4 \pm 8.3 \pm 4.8	47.1 \pm 8.0 \pm 5.9
1.29	45.2 \pm 7.9 \pm 4.5	40.3 \pm 7.6 \pm 7.1	42.1 \pm 7.6 \pm 3.6	40.1 \pm 5.5 \pm 3.9	43.0 \pm 6.4 \pm 3.6	35.0 \pm 8.2 \pm 5.0
1.31	29.7 \pm 7.0 \pm 15.2	18.0 \pm 5.9 \pm 5.4	42.3 \pm 6.0 \pm 2.4	37.0 \pm 5.0 \pm 3.1	41.4 \pm 7.7 \pm 3.5	43.7 \pm 11.4 \pm 7.7
1.33	41.6 \pm 8.1 \pm 10.4	33.0 \pm 6.1 \pm 3.1	39.7 \pm 4.8 \pm 3.2	31.1 \pm 5.1 \pm 3.4	28.8 \pm 8.0 \pm 6.5	20.9 \pm 8.6 \pm 1.4
1.35	19.9 \pm 4.8 \pm 4.4	21.2 \pm 4.2 \pm 4.4	30.2 \pm 4.0 \pm 2.1	35.1 \pm 6.6 \pm 6.7	27.1 \pm 8.3 \pm 8.0	23.9 \pm 8.8 \pm 5.4
1.37	17.5 \pm 4.1 \pm 4.3	21.6 \pm 3.7 \pm 2.1	30.5 \pm 4.6 \pm 2.4	11.8 \pm 5.0 \pm 9.5	24.4 \pm 7.3 \pm 2.1	22.5 \pm 9.6 \pm 8.2
1.39	18.0 \pm 3.8 \pm 3.1	24.2 \pm 3.9 \pm 4.0	18.5 \pm 4.7 \pm 4.4	23.5 \pm 5.8 \pm 4.8	29.1 \pm 8.5 \pm 6.8	33.0 \pm 11.6 \pm 3.0
1.41	23.0 \pm 4.3 \pm 1.3	20.3 \pm 4.2 \pm 2.0	19.8 \pm 5.1 \pm 4.8	31.8 \pm 6.2 \pm 5.1	24.7 \pm 7.8 \pm 3.6	32.7 \pm 10.0 \pm 4.4
1.43	23.9 \pm 4.8 \pm 2.3	20.8 \pm 5.0 \pm 5.3	16.8 \pm 4.5 \pm 3.0	21.6 \pm 5.6 \pm 2.4	33.7 \pm 8.0 \pm 4.7	27.0 \pm 8.5 \pm 5.5
1.45	15.6 \pm 4.9 \pm 4.1	24.8 \pm 6.1 \pm 3.2	30.8 \pm 5.8 \pm 2.2	33.4 \pm 6.6 \pm 4.5	36.7 \pm 7.3 \pm 5.1	45.5 \pm 10.4 \pm 6.7
1.47	34.3 \pm 7.4 \pm 2.9	33.8 \pm 6.5 \pm 3.6	37.0 \pm 6.2 \pm 2.3	37.5 \pm 6.0 \pm 4.9	44.8 \pm 8.0 \pm 6.0	39.4 \pm 10.5 \pm 4.6
1.49	41.5 \pm 7.8 \pm 4.0	41.5 \pm 6.8 \pm 4.2	45.5 \pm 6.3 \pm 8.8	45.4 \pm 5.9 \pm 7.0	64.1 \pm 9.5 \pm 10.3	67 \pm 11 \pm 10
1.51	36.5 \pm 6.7 \pm 4.6	36.6 \pm 6.1 \pm 4.0	48.6 \pm 5.6 \pm 5.9	50.8 \pm 6.1 \pm 5.8	47.6 \pm 7.4 \pm 5.2	85 \pm 11 \pm 11
1.53	39.8 \pm 6.7 \pm 4.7	39.9 \pm 6.0 \pm 5.4	37.0 \pm 4.9 \pm 4.6	42.4 \pm 5.6 \pm 4.5	39.9 \pm 6.2 \pm 3.7	50.4 \pm 8.7 \pm 6.3
1.55	37.1 \pm 6.3 \pm 2.5	31.4 \pm 4.8 \pm 3.9	26.8 \pm 4.0 \pm 4.6	39.0 \pm 4.9 \pm 3.6	57.8 \pm 7.0 \pm 5.2	61.1 \pm 10.0 \pm 7.1
1.57	15.6 \pm 3.9 \pm 3.8	19.7 \pm 3.8 \pm 3.5	32.7 \pm 4.1 \pm 2.8	36.8 \pm 4.3 \pm 3.2	41.3 \pm 6.9 \pm 7.3	31.7 \pm 9.2 \pm 10.2
1.59	18.5 \pm 3.9 \pm 1.3	30.0 \pm 4.2 \pm 3.1	31.5 \pm 3.8 \pm 3.5	40.1 \pm 4.7 \pm 4.7	27.8 \pm 6.4 \pm 5.0	26.0 \pm 7.2 \pm 8.9
1.61	18.1 \pm 3.7 \pm 3.4	21.7 \pm 3.7 \pm 3.5	28.9 \pm 3.5 \pm 3.7	23.8 \pm 4.5 \pm 3.5	31.8 \pm 5.9 \pm 2.4	26.2 \pm 6.4 \pm 4.0
1.63	19.0 \pm 4.0 \pm 2.2	26.4 \pm 3.8 \pm 1.8	29.4 \pm 3.8 \pm 2.6	27.0 \pm 4.4 \pm 4.3	32.6 \pm 5.2 \pm 4.2	35.8 \pm 6.7 \pm 2.7
1.65	20.4 \pm 4.1 \pm 3.3	25.1 \pm 3.7 \pm 2.2	22.3 \pm 3.6 \pm 3.8	29.2 \pm 3.8 \pm 2.4	39.5 \pm 5.6 \pm 5.0	36.8 \pm 7.5 \pm 6.8
1.67	17.7 \pm 3.6 \pm 3.4	16.2 \pm 3.2 \pm 1.6	26.1 \pm 3.5 \pm 2.2	18.8 \pm 3.1 \pm 2.4	17.0 \pm 5.3 \pm 4.7	19.7 \pm 8.3 \pm 3.2
1.69	10.8 \pm 3.2 \pm 2.6	16.2 \pm 3.4 \pm 3.6	21.5 \pm 3.0 \pm 4.5	16.0 \pm 3.6 \pm 2.9	30 \pm 13 \pm 26	22.4 \pm 14.6 \pm 9.8
1.71	13.1 \pm 3.7 \pm 3.8	13.3 \pm 3.1 \pm 1.5	14.1 \pm 2.6 \pm 3.5	8.9 \pm 4.3 \pm 1.9	16.8 \pm 5.6 \pm 2.3	9.5 \pm 5.0 \pm 2.5
1.73	3.4 \pm 2.4 \pm 3.0	6.2 \pm 2.4 \pm 4.5	8.4 \pm 2.8 \pm 2.0	14.4 \pm 3.6 \pm 2.0	16.7 \pm 3.4 \pm 3.4	14.3 \pm 3.7 \pm 2.3
1.75	17.2 \pm 3.5 \pm 2.0	6.5 \pm 2.5 \pm 1.9	11.1 \pm 3.3 \pm 1.3	10.3 \pm 2.2 \pm 2.6	6.7 \pm 2.4 \pm 1.3	8.2 \pm 3.0 \pm 1.4
1.77	4.2 \pm 2.9 \pm 5.4	5.1 \pm 2.5 \pm 0.9	7.1 \pm 2.2 \pm 1.7	8.0 \pm 1.7 \pm 1.0	8.0 \pm 2.4 \pm 2.3	11.6 \pm 3.4 \pm 1.6
1.79	5.6 \pm 2.6 \pm 3.3	9.6 \pm 2.6 \pm 1.8	7.0 \pm 1.6 \pm 1.8	8.4 \pm 1.7 \pm 0.8	3.7 \pm 4.0 \pm 3.5	4.6 \pm 4.0 \pm 3.5
1.81	4.9 \pm 2.0 \pm 2.0	8.8 \pm 2.0 \pm 0.9	7.9 \pm 1.5 \pm 0.8	13.6 \pm 2.2 \pm 3.1	19.0 \pm 9.3 \pm 10.8	18.6 \pm 9.3 \pm 9.8
1.83	8.2 \pm 1.9 \pm 1.1	5.7 \pm 1.6 \pm 1.1	7.7 \pm 1.6 \pm 0.9	5.6 \pm 3.1 \pm 5.1	4.9 \pm 3.6 \pm 2.1	7.1 \pm 4.3 \pm 2.8
1.85	4.6 \pm 1.7 \pm 0.9	8.4 \pm 1.8 \pm 1.5	5.6 \pm 1.8 \pm 1.7	7.3 \pm 2.4 \pm 1.1	9.2 \pm 2.7 \pm 1.0	8.3 \pm 3.2 \pm 2.2
1.87	4.6 \pm 1.9 \pm 1.2	4.8 \pm 2.1 \pm 1.2	5.4 \pm 2.0 \pm 1.6	6.4 \pm 1.8 \pm 0.8	7.1 \pm 2.3 \pm 2.3	6.6 \pm 2.9 \pm 1.4
1.89	8.1 \pm 3.5 \pm 11.2	8.7 \pm 2.6 \pm 2.2	8.2 \pm 1.8 \pm 0.9	5.8 \pm 1.6 \pm 1.0	13.5 \pm 2.9 \pm 2.8	7.8 \pm 3.6 \pm 1.9
1.91	10.1 \pm 2.6 \pm 1.9	4.2 \pm 2.7 \pm 1.8	5.0 \pm 1.4 \pm 1.2	7.3 \pm 1.8 \pm 1.8	5.7 \pm 3.7 \pm 1.8	10.0 \pm 5.9 \pm 3.9

[23] G. A. Miller, Phys. Rev. **C69**, 052201 (2004).Nucl. Phys. **A645**, 145 (1999).

[24] D. Drechsel, O. Hanstein, S. S. Kamalov, and L. Tiator,

TABLE II: $ep \rightarrow ep\gamma$ cross section (\pm stat \pm syst) at $Q^2=1.0$ GeV² and $\cos\theta_{\gamma\gamma}^* = -0.875$, in fm/MeV/sr².

$W(\text{GeV})$	$\phi = 15^\circ$	$\phi = 45^\circ$	$\phi = 75^\circ$	$\phi = 105^\circ$	$\phi = 135^\circ$	$\phi = 165^\circ$
0.99	103 \pm 74 \pm 21	548 \pm 306 \pm 112	362 \pm 159 \pm 75	459 \pm 107 \pm 63	453 \pm 78 \pm 46	478 \pm 71 \pm 39
1.01	76 \pm 43 \pm 10	230 \pm 94 \pm 94	320 \pm 75 \pm 54	342 \pm 54 \pm 30	361 \pm 47 \pm 42	291 \pm 37 \pm 28
1.03	65 \pm 27 \pm 14	186 \pm 60 \pm 26	263 \pm 48 \pm 33	224 \pm 34 \pm 17	280 \pm 34 \pm 20	282 \pm 32 \pm 22
1.05	41 \pm 24 \pm 17	144 \pm 43 \pm 13	204 \pm 35 \pm 23	197 \pm 28 \pm 14	144 \pm 22 \pm 18	141 \pm 21 \pm 11
1.07	22.2 \pm 16.2 \pm 2.0	124 \pm 34 \pm 18	87.7 \pm 19.6 \pm 9.0	154 \pm 22 \pm 12	134.5 \pm 19.4 \pm 6.5	157 \pm 20 \pm 14
1.09	16.9 \pm 12.1 \pm 4.5	115 \pm 29 \pm 10	143.9 \pm 23.4 \pm 9.5	96 \pm 16 \pm 40	124 \pm 17 \pm 14	121 \pm 19 \pm 11
1.11	30.7 \pm 15.7 \pm 7.7	69.9 \pm 20.7 \pm 4.2	106.7 \pm 18.4 \pm 8.3	134 \pm 18 \pm 10	129 \pm 21 \pm 13	81 \pm 20 \pm 45
1.13	30.1 \pm 14.1 \pm 5.2	85.5 \pm 20.1 \pm 8.1	82.8 \pm 14.8 \pm 6.6	114.0 \pm 17.9 \pm 4.5	78 \pm 19 \pm 16	105 \pm 30 \pm 11
1.15	59.7 \pm 20.1 \pm 3.9	45 \pm 13 \pm 12	133.1 \pm 19.0 \pm 9.7	99 \pm 18 \pm 18	98 \pm 22 \pm 13	116 \pm 25 \pm 10
1.17	31.1 \pm 14.1 \pm 8.2	43 \pm 14 \pm 15	110.2 \pm 17.7 \pm 5.1	107 \pm 18 \pm 11	118 \pm 22 \pm 14	106 \pm 30 \pm 14
1.19	130 \pm 28 \pm 26	118.5 \pm 18.9 \pm 8.4	123 \pm 17 \pm 11	126 \pm 18 \pm 12	145 \pm 29 \pm 18	272 \pm 122 \pm 90
1.21	103 \pm 21 \pm 11	124.6 \pm 19.0 \pm 7.2	135.7 \pm 17.5 \pm 5.5	183 \pm 21 \pm 11	177 \pm 51 \pm 18	217 \pm 70 \pm 46
1.23	129.0 \pm 21.1 \pm 8.7	117.4 \pm 18.5 \pm 6.7	135.2 \pm 16.3 \pm 9.8	133 \pm 20 \pm 12	130 \pm 24 \pm 42	68 \pm 19 \pm 28
1.25	99.1 \pm 17.4 \pm 6.2	95.9 \pm 17.8 \pm 7.0	99.2 \pm 13.4 \pm 7.4	68.2 \pm 14.1 \pm 8.3	88 \pm 14 \pm 14	81.8 \pm 21.3 \pm 8.8
1.27	54.1 \pm 13.9 \pm 7.6	60 \pm 13 \pm 14	87.1 \pm 13.2 \pm 5.6	71.3 \pm 11.8 \pm 6.3	58.0 \pm 12.5 \pm 7.3	
1.29	35.6 \pm 11.8 \pm 5.7	41.8 \pm 10.1 \pm 9.8	47.8 \pm 10.0 \pm 4.1	70.0 \pm 9.4 \pm 4.7	58.5 \pm 19.2 \pm 7.6	
1.31	29.6 \pm 10.7 \pm 5.7	51.8 \pm 10.7 \pm 5.9	49.2 \pm 9.0 \pm 3.1	58.3 \pm 8.8 \pm 3.7		
1.33	29.3 \pm 8.5 \pm 2.5	44.8 \pm 10.4 \pm 4.7	35.0 \pm 6.6 \pm 4.3	39.8 \pm 8.8 \pm 2.7		
1.35	10.4 \pm 5.0 \pm 7.7	28.9 \pm 9.7 \pm 4.6	31.2 \pm 5.4 \pm 3.3	42 \pm 11 \pm 10		
1.37	24.0 \pm 9.9 \pm 5.9	57.9 \pm 12.3 \pm 5.0	45.0 \pm 6.3 \pm 4.1	38.4 \pm 12.4 \pm 4.1		
1.39		42.1 \pm 7.5 \pm 7.4	35.9 \pm 6.2 \pm 2.3	31.8 \pm 10.3 \pm 6.8		
1.41		21.3 \pm 4.8 \pm 7.8	30.8 \pm 6.9 \pm 1.8	18.0 \pm 9.1 \pm 4.1		
1.43		32.1 \pm 5.7 \pm 4.2	27.6 \pm 8.0 \pm 6.6	25.8 \pm 11.0 \pm 7.0		
1.45		36.9 \pm 7.3 \pm 8.8	31.3 \pm 8.6 \pm 5.5	11.4 \pm 8.4 \pm 10.1		
1.47		44.4 \pm 11.7 \pm 8.6	25.3 \pm 7.9 \pm 10.7	49.3 \pm 12.4 \pm 9.3		
1.49		47 \pm 13 \pm 14	46.8 \pm 10.0 \pm 6.9	70.4 \pm 14.3 \pm 8.9		
1.51		38.4 \pm 10.8 \pm 6.5	57.1 \pm 10.6 \pm 5.7	50 \pm 12 \pm 16		
1.53		40.5 \pm 11.4 \pm 6.8	53.4 \pm 10.0 \pm 3.4	37 \pm 10 \pm 12		
1.55		30 \pm 13 \pm 16	45.2 \pm 8.4 \pm 2.6	42.0 \pm 10.9 \pm 6.5		
1.57		10.3 \pm 8.8 \pm 1.8	36.7 \pm 7.8 \pm 6.8	59.3 \pm 12.3 \pm 5.2		
1.59		15.5 \pm 7.3 \pm 9.9	22.1 \pm 6.7 \pm 3.6	37.2 \pm 12.6 \pm 4.3		
1.61		12.8 \pm 6.7 \pm 6.5	28.4 \pm 7.4 \pm 3.3	30.8 \pm 11.8 \pm 3.7		
1.63			47.3 \pm 9.1 \pm 4.3	32.9 \pm 12.4 \pm 6.7		
1.65			48.9 \pm 9.7 \pm 6.0	27.3 \pm 14.4 \pm 5.3		
1.67			18.1 \pm 7.4 \pm 7.1	47 \pm 13 \pm 15		

TABLE III: $ep \rightarrow ep\gamma$ cross section (\pm stat \pm syst) at $Q^2=1.0$ GeV² and $\cos\theta_{\gamma\gamma}^* = -0.650$, in fm/MeV/sr².

$W(\text{GeV})$	$\phi = 15^\circ$	$\phi = 45^\circ$	$\phi = 75^\circ$	$\phi = 105^\circ$	$\phi = 135^\circ$	$\phi = 165^\circ$
0.99			554 \pm 216 \pm 88	452 \pm 90 \pm 38	454 \pm 64 \pm 23	340 \pm 49 \pm 26
1.01			380 \pm 87 \pm 71	286 \pm 46 \pm 17	213 \pm 30 \pm 16	274 \pm 31 \pm 17
1.03		237 \pm 109 \pm 55	270 \pm 50 \pm 18	195 \pm 28 \pm 16	233 \pm 27 \pm 12	205 \pm 25 \pm 11
1.05		277 \pm 94 \pm 63	234 \pm 41 \pm 12	211 \pm 27 \pm 16	167 \pm 22 \pm 14	173.9 \pm 22.2 \pm 9.6
1.07		65 \pm 36 \pm 19	183.2 \pm 29.7 \pm 8.7	161 \pm 21 \pm 10	140 \pm 18 \pm 11	142 \pm 19 \pm 20
1.09		266 \pm 59 \pm 12	153.9 \pm 24.0 \pm 9.5	169.1 \pm 20.6 \pm 9.2	138 \pm 19 \pm 10	97 \pm 21 \pm 101
1.11		189 \pm 44 \pm 18	139.0 \pm 21.1 \pm 5.3	108.1 \pm 15.8 \pm 7.7	152 \pm 26 \pm 41	
1.13	462 \pm 181 \pm 270	195.4 \pm 41.0 \pm 9.0	113.5 \pm 17.1 \pm 5.6	123.1 \pm 18.8 \pm 7.5		
1.15	131 \pm 69 \pm 97	92.1 \pm 26.4 \pm 9.9	102.4 \pm 15.6 \pm 5.4	125 \pm 20 \pm 11		
1.17		132 \pm 27 \pm 13	95 \pm 15 \pm 10	135 \pm 21 \pm 15		
1.19		107 \pm 22 \pm 24	168.7 \pm 20.3 \pm 5.9	152 \pm 22 \pm 27		
1.21		154 \pm 24 \pm 22	153 \pm 18 \pm 14	125 \pm 21 \pm 17		
1.23		104 \pm 19 \pm 16	132 \pm 17 \pm 10	87 \pm 21 \pm 10		
1.25		108 \pm 19 \pm 12	76 \pm 13 \pm 12	50 \pm 15 \pm 59		
1.27		107 \pm 20 \pm 11	103 \pm 15 \pm 15	85 \pm 16 \pm 73		
1.29		51.1 \pm 17.4 \pm 6.8	79 \pm 15 \pm 15	43 \pm 10 \pm 12		
1.31		77 \pm 19 \pm 23	69 \pm 13 \pm 14	68 \pm 14 \pm 32		
1.33		60 \pm 16 \pm 16	42 \pm 10 \pm 15	54 \pm 15 \pm 42		
1.35		62.7 \pm 16.3 \pm 4.4	65.6 \pm 11.4 \pm 3.4			